Electrical characteristics and electron heating mechanism of an inductively coupled argon discharge

V A Godyak, R B Piejak and B M Alexandrovich

Osram Sylvania Inc., 100 Endicott Street, Danvers, MA 01923, USA

Abstract. The external electrical characteristics of inductively coupled argon RF discharges at 13.56 MHz have been measured over a wide range of power at gas pressures ranging from 3 mTorr to 3 Torr. External parameters, such as coil voltage, current and phase shift, were measured. From these measurements the equivalent discharge resistance and reactance, the power transfer efficiency and the coupling coefficient between the primary coil and the plasma were determined as a function of discharge power and gas pressure. The efficient RF power transfer and the large value of the effective electron collision frequency found here at low gas pressure suggest some collisionless electron heating mechanisms. This mechanism is identified as non-local electron heating in the inhomogeneous RF field due to spatial dispersion of the plasma conductivity.

1. Introduction

Low-pressure inductively coupled RF discharge sources have important industrial applications mainly because they can provide a high-density electrodeless plasma source with low ion energy and low power loss in the sheaths. These attractive features of inductively coupled discharges are recognized by both the plasma processing and the lighting community and therefore the study of these types of discharges has been actively pursued, especially over recent years.

Although inductive discharges are being vigorously studied [1–4], few data can be found in the literature about the external electrical characteristics of the induction coil that drives the discharge. This is not to say that voltage and current measurements of the induction coil for a specific point cannot be found in the literature but that a comprehensive set of measurements over a wide range of inductive discharges operation is indeed unavailable. A comprehensive set of measurements could provide a basis for the development of scaling laws for the external and internal discharge characteristics from which control of RF discharges and optimization of plasma processes could be achieved. The measurement of discharge and plasma parameters over a wide range of external conditions given here is valuable for inductive RF discharge modelling and possibly as a database for comparison of theory with experiment.

The objective of this work is to report on measurements of the external electrical characteristics of an inductively coupled discharge over a wide range of operating parameters. Measurements of the voltage, current and phase shift on the primary coil of an inductive discharge have been made over a range of power between about 20 W and 180 W and over a range of argon gas pressure between 3 Torr, where electron–neutral (e–n) collisions dominate, and 3 mTorr where e–n collisons are considerably reduced. From these measurements, the resistive (ohmic) and reactive components of the primary coil impedance, the power transfer efficiency, the minimal maintenance power and the effective electron collision frequency have been determined based on an approach developed by Piejak *et al* [4]. At low gas pressure, the effective electron collision frequency has been shown to exceed the electron–atom collision frequency considerably, suggesting that a collisionless dissipative process is responsible for electron heating. This heating is shown to be the result of spatial dispersion of the plasma conductivity in an inhomogeneous RF field, a phenomenon underlying the anomalous skin effect. The estimation of the effective electron collision frequency based on this concept is in reasonable agreement with experiment.

2. Experimental set-up

Measurements were made in a discharge chamber formed by a glass cylinder with an ID of 14.3 cm and an OD of 15.0 cm and limited at each end of the cylinder by aluminium plates 6.7 cm apart. A sketch of the discharge vessel and location of the discharge induction (primary) coil is shown in figure 1(*a*). All measurements were made with argon gas flow to enhance gas purity. The discharge chamber and vacuum–gas flow system have been described elsewhere [5]. This set-up varies from previ-
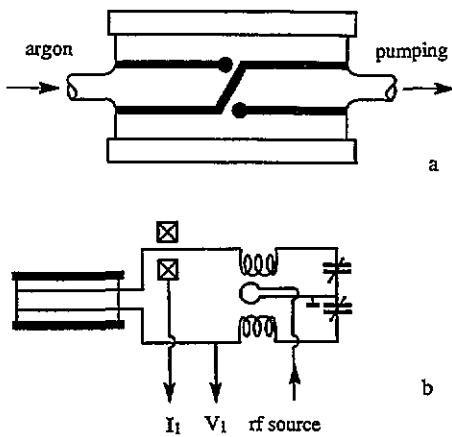
Figure 1. (a) A diagram of the experimental test chamber consisting of a glass cylinder about which a two-turn coil is wound bounded by aluminium upper and lower plates. (b) A simplified schematic diagram of the symmetrical matching system attached to an induction coil. Measurement points for discharge voltage, current and transmitted power are indicated.

ous work [4] in that the induction coil is attached to the exterior of the glass cylinder. The induction coil consists of two turns of 0.3 cm wide copper foil strip separated by 2.0 cm and is connected as shown in figure 1. With the coil and aluminium plates positioned as shown and no plasma present, the effective inductance L_0 and resistance R_0 of the unloaded coil (including leads to the matching system) were measured at 13.56 MHz and found to be 0.84 μH and 0.65 Ω respectively. In this paper the inductor with plasma present (loaded) will be referred to as the primary coil, otherwise (with no plasma) it will be referred to as the unloaded coil. Note that the aluminium plates reduce the initial coil inductance by about 15% suggesting that the RF field is localized about the coil winding and loosely coupled to the plates.

A simplified schematic diagram of the matcher circuit showing the electrical measurement points is given in figure 1(b). The source of discharge power is an RF amplifier that delivers power to a link coupled matching system. The secondary coils of the matcher are arranged so as to form a symmetric (push–pull with respect to ground) source of RF power for the induction coil and discharge. For a given discharge current, a symmetric source reduces the capacitive coupling which may affect the electrical characteristics of the discharge, especially at low RF power. The RF voltage is measured with a voltage divider directly at the input of the induction coil and current is measured with a current transformer as shown in figure 1(b). These measurements are made with a vector voltmeter in which the phase shift between the current and voltage is also measured. The incident and reflected powers are also measured in the line between the RF source and the matcher. In conjunction with a calibration curve to account for matcher losses [6], these measurements serve as an independent check of the power determined from the vector voltmeter

measurements. The agreement between the two measurement techniques is generally within a few per cent. Errors in voltage and current measurements in this system [5–7] are less than or equal to about 5% while error in relative phase shift is about 0.1° which corresponds to about a 10% error in the worst case of the smallest power factor ($\cos \phi = 0.02$) measured in this work.

3. Measurement results

The primary current of the induction coil against total power is shown in figure 2. Only data for two gas pressures are shown in this figure but these data are qualitatively representative of discharge behaviour at all gas pressure and power levels considered here. At a fixed gas pressure the primary current increases with power while at a given power level the primary current is smaller at the higher gas pressure. The RF voltage across the primary coil against the total power is shown in figure 3. The trends in coil voltage against power are qualitatively similar to that of the coil current. The power factor for these two gas pressures is shown in figure 4. In all cases the power factor increases more rapidly with power at lower power levels and less rapidly at higher power levels. At a given power level, the power factor increases with gas pressures.

The external electrical characteristics of an inductive discharge may be given in terms of the equivalent coil resistance and reactance against total RF power. The primary coil resistance against total power is shown in figure 5. At each gas pressure the equivalent resistance of the primary coil increases with power and reaches a plateau at the higher gas pressures. For a fixed power, the primary resistance increases with gas pressure. The increase in equivalent resistance represents coupling of the plasma resistance into the primary coil circuit and is fundamental in the power transfer from the primary coil to the secondary (plasma) of an air coil transformer. Since with increasing power the resistance of the pri-
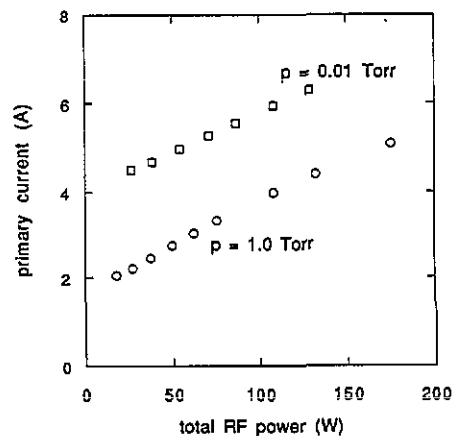

Figure 2. Current (RMS) through the primary induction coil as a function of the total RF power delivered to the coil for gas pressures of 0.01 and 1.0 Torr.
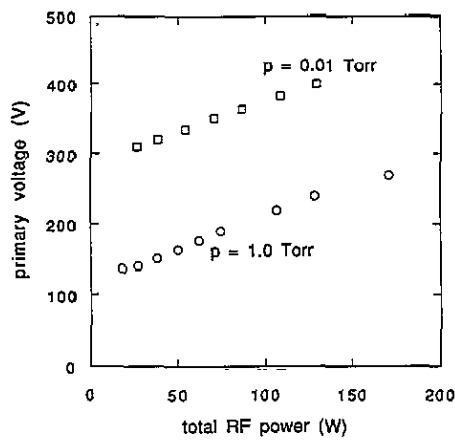
Figure 3. Voltage (RMS) across the primary coil as a function of the total RF power delivered to the coil for gas pressures of 0.01 and 1.0 Torr.
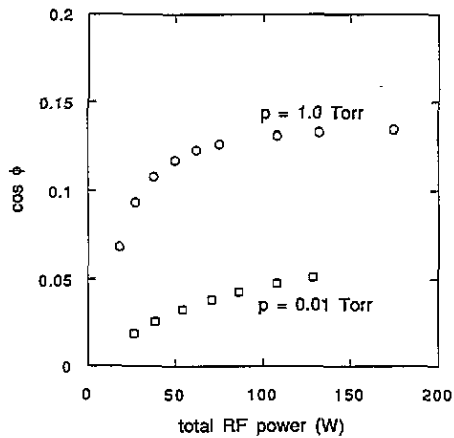

Figure 4. Power factor against total RF power over a power range between 20 and 180 W.
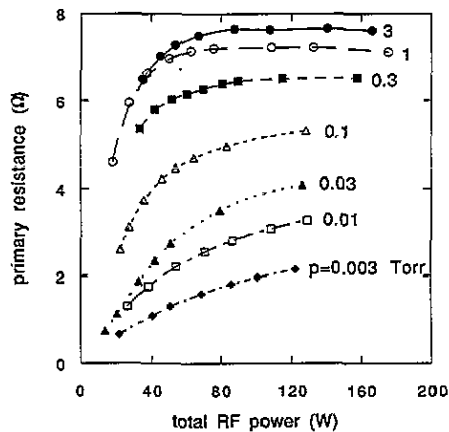

Figure 5. Primary resistance against total RF power for argon gas pressures between 3 mTorr and 3 Torr.

mary coil itself R_0 is virtually constant, the increase in primary resistance is directly related to an increase in the power transferred to the plasma.

The equivalent primary coil reactance versus power is given in figure 6. At a fixed gas pressure the primary reactance decreases with total power while at a fixed power level the primary reactance decreases with increasing gas pressure. As in the case of equivalent resistance the reduction in primary reactance reflects an
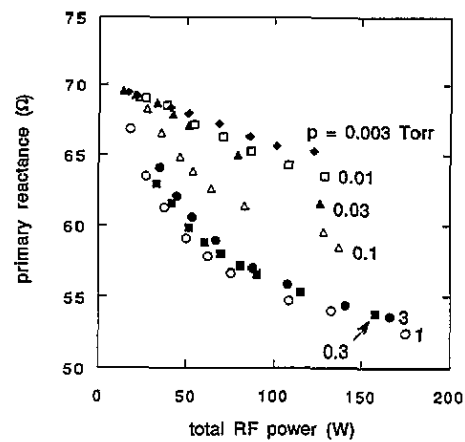

Figure 6. Primary coil reactance against total RF power for argon gas pressures between 3 mTorr and 3 Torr.

increase in the mutual coupling between the coil and the plasma. Essentially, the plasma current flow partially *neutralizes the time varying magnetic flux created by* current flow through the primary coil. Thus, a reduction in the primary equivalent reactance represents the diamagnetic effect of the plasma coupled to the primary coil.

4. Evaluation of internal discharge parameters

From direct measurements of the external electrical characteristics of the discharge, spatially integrated internal discharge parameters can be inferred [4]. These parameters are the power dissipated in the plasma P_2, the minimal inductive discharge power P_0, the coupling coefficient k between the primary coil and the plasma and the Q factor of the secondary (plasma) circuit Q_2 (which is the ratio between the reactance and the resistance of the secondary circuit including the plasma). Some of these parameters are unique functions of external (given) discharge parameters: geometry, frequency, gas type and pressure and total RF power while others may be expressed as an average over a certain RF power range or over the range of another external parameter. The basis for inferring these internal parameters is the transformer theory equations (see, for example the work of Piejak *et al* [4]) which in essence are spatial integrals of *Maxwell's equations*:

$$\rho = R_1 - R_0 = \omega^2 k^2 L_0 L_2 R_2 / Z_2^2 \qquad (1)$$

$$\zeta = \omega(L_0 - L_1) = \omega^2 k^2 L_0 L_2 (\omega L_2 + \omega/\nu_{eff} R_2)/Z_2^2 \quad (2)$$

where ρ and ζ correspond to changes in primary resistance and reactance (for a series equivalent circuit) due to plasma loading; R_0 and $\omega L_0 = X_0$ correspond to the unloaded coil resistance and reactance; R_1 and ωL_1 correspond to the primary resistance and reactance with plasma; L_2 and R_2 are the magnetic inductance and ohmic resistance (plasma resistance) of the secondary circuit; $Z_2 = [\omega L_2 + \omega/\nu_{eff} R_2)^2 + (R_2)^2]^{1/2}$ is the impedance of the secondary circuit; and ν_{eff} is the effective

electron collision frequency accounting for RF power dissipation process in the inductive RF plasma [4].

Expressions for k, Q_2 and P_2 directly follow from equations (1) and (2):

$$k^2 = (\zeta^2 + \rho^2)/X_0(\zeta - \rho\omega/v_{\text{eff}}) \qquad (3)$$

$$Q_2 \equiv \omega L_2/R_2 + \omega/v_{\text{eff}} = \zeta/\rho \qquad (4)$$

$$P_2 = I^2\rho. \qquad (5)$$

From the measured external electrical parameters these parameters can be found for each point of discharge operation. Moreover, they can be found for any arbitrary inductive RF discharge, without prior knowledge of a particular discharge geometry or spatial distribution of plasma and the electromagnetic field.

In our experimental arrangement the aluminium end plates affect the unloaded coil inductance to an extent comparable to that caused by the plasma. However, since the plate conductivity and position referenced to the unloaded coil remains unchanged throughout the experiment, the influence of the plates is accounted for in the unloaded coil characteristic constants X_0 and R_0 (measured with the plates and no plasma). Only in a strong skin effect regime, when RF field distribution is significantly affected by the plasma, might one expect some change in X_0 and R_0, however, as will be shown, this case is not encountered in these experiments.

Having inferred RF power absorbed by the plasma P_2, power transfer efficiency η is simply P_2/P_1. Figure 7 represents η as a function of the total RF power P_1 for argon pressure between 3 mTorr and 3 Torr. In general, $\eta(P_1)$ drops at small and decreasing P_1 as P_1 approaches the minimal maintenance power P_0 (dissipated in the unloaded coil, $P_0 = I_1^2 R_0$ as $P_2 \to 0$) needed to induce an RF electric field sufficient to maintain the plasma. As shown by Piejak $et\ al$

$$P_0 = (1 + \omega^2/v_{\text{eff}}^2)V_2^2/k^2 Q_0 \omega L_2 \qquad (6)$$

where $V_2 = (P_2 R_2)^{1/2}$ is the ohmic component of the secondary voltage and Q_0 is the Q factor of the unloaded primary coil. P_0 varies with gas pressure, since the ohmic component of plasma voltage V_2 (governed by ionization and energy balance) as well as the factor ω/v_{eff} depend on the gas pressure. The minimal maintenance power P_0 is the power in the primary coil in the limit $P_2 \to 0$ and can be found from the measurements of the primary current I_1 as $P_0 = I_{10}^2 R_0$, where $I_{10} = I_1$ as $P_2 \to 0$.

In figure 8 the primary current I_1 is shown as a function of the discharge power P_2 for different argon pressures. Extrapolating $I_1(P_2)$ to the limit $P_2 = 0$ gives an estimate of I_{10} and P_0. From figure 8 for $p = 1.0$, 0.1, 0.01 and 0.003 Torr the corresponding values of I_{10} are 1.7, 2.5, 4.2, and 5.7 A, resulting in a minimal maintenance power P_0 of 1.9, 4.0, 11.5, and 21 W respectively. Thus, as shown in [4], power loss in the primary coil generally increases with decreasing gas pressure thereby reducing power transfer efficiency to the plasma load. As one can see in figure 7 the power transfer efficiency grows with RF power, and according to [4] reaches a broad maximum at the condition when the secondary magnetic reactance equals the plasma impedance:

$$\omega L_2 = R_2(1 + \omega^2/v_{\text{eff}}^2)^{1/2}. \qquad (7)$$

It seems (from figure 7) that such a condition is reached for relatively large argon pressure ($p = 0.3$–3 Torr) where collisionally dominated electron heating processes occur through electron–atom collisions ($v_{\text{eff}} = v_{\text{en}}$) and $\omega^2/v_{\text{en}}^2 \ll 1$, where v_{en} is the electron–atom collision frequency. At these pressures RF power is efficiently transferred to the plasma over a wide range of total RF power and $\eta \approx 0.9$. At lower argon pressure ($p = 3$–30 mTorr) η is somewhat smaller ($\eta = 0.4$–0.8) but does not drop as dramatically as expected [4] for collisional heating and $\omega^2/v_{\text{en}}^2 \gg 1$.

Preliminary probe measurements of the electron energy distribution function in this discharge at $p = 10$ mTorr allowed us to estimate (using the electron–atom cross section for argon) the electron–atom collision frequency $v_{\text{en}} \approx 2.0 \times 10^6$ s^{-1} suggesting that $\omega/v_{\text{en}} \approx$
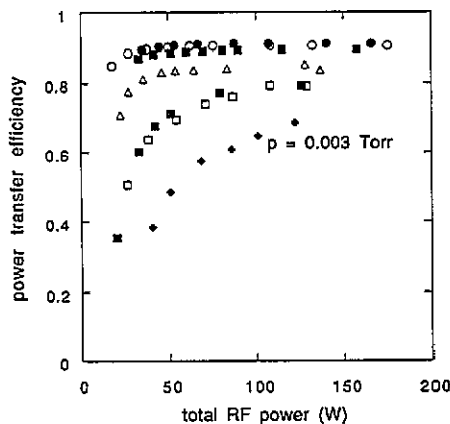

Figure 7. Power transfer efficiency against total RF power for argon gas pressures between 3 mTorr and 3 Torr. The symbols for pressure are the same as in the previous figures.
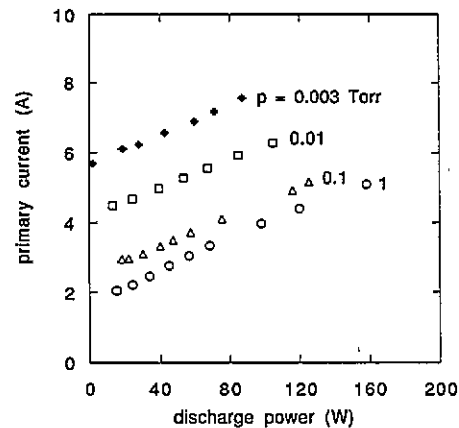

Figure 8. The primary RF current against discharge power for $p = 0.003$, 0.01, 0.1 and 1 Torr.

40. For this value of ω/ν_{en} one can then obtain [4] the power transfer efficiency:

$$\eta \leqslant (1 + 4k^{-2}Q_0^{-1}\omega/\nu_{en})^{-1} = 0.25 \qquad (8)$$

where the sign of equality on the left-hand side of expression (8) corresponds to the matching condition (7).

Assuming a collisional electron heating process at $p = 10$ mTorr, η should be no more than 0.25, whereas experimental data plotted in figure 7 show much larger values of η (up to $\eta = 0.8$). An even larger difference between collisional and experimental values of η is expected for $p = 3$ mTorr. Thus, at low pressure there is some additional non-collisional dissipation process, such that $\nu_{eff} > \nu_{en}$.

5. Effective electron collision frequency

It appears to be possible to infer the value of ν_{eff} from measured electrical characteristics of the primary coil using equation (4), although the parameter $\omega L_2/R_2$ in this equation remains unknown. This can be done in a number of ways. First, the ratio ω/ν_{eff} can be found at the specific value of P_1 corresponding to the matching condition (7) when the power transfer efficiency $\eta(P_1)$ is maximal:

$$\omega/\nu_{eff} = 1/2(\zeta/\rho - \rho/\zeta). \qquad (9)$$

Unfortunately, at low pressure, the matching condition does not appear to be reached within the RF power interval of the present experiment. Another way to find ν_{eff} is at the condition when $\omega L_2/R_2 \ll \omega/\nu_{eff}$ which occurs in the limit of small discharge power P_2. Noting that $R_2 = V_2^2 P_2^{-1}$, equation (4) may be rewritten in the following form:

$$\zeta/\rho = \omega L_2 P_2/V_2^2 + \omega/\nu_{eff} = Q_2 \qquad (10)$$

from where in the limit as $P_2 \to 0$ one obtains:

$$\omega/\nu_{eff} = \zeta/\rho. \qquad (11)$$

Experimental values of $Q_2 = \zeta/\rho$ are given in figure 9 as functions of the discharge power P_2 for $p = 10$ mTorr and 1.0 Torr. Extrapolation of the experimental data of ζ/ρ for $p = 10$ mTorr to the point where $P_2 = 0$ yields a value of $\omega/\nu_{eff} = 2.2$ corresponding to $\nu_{eff} = 3.9 \times 10^7$ s^{-1} which is more than an order of magnitude larger than the electron–atom collision frequency ν_{en}. The corresponding calculation for $p = 3$ mTorr gives $\nu_{eff} \approx 2.0 \times 10^7$ s^{-1} which also greatly exceeds ν_{en} at this pressure. As seen in figure 9, at $p = 10$ mTorr, ζ/ρ grows linearly with P_2 inferring, according to equation (10), that the ratio $\omega L_2/V_2^2$ is nearly constant. This seems reasonable since both L_2 which is governed by the RF field and plasma distributions and V_2 which is proportional to the plasma RF field, are nearly independent of P_2 at low gas pressures.

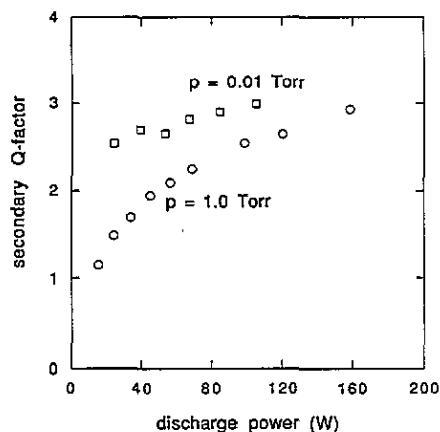A different behaviour for ζ/ρ with P_2 is seen for $p = 1.0$ Torr. Although as expected for $\omega/\nu_{en} \ll 1$,

Figure 9. The Q factor of the secondary circuit against the discharge power for 0.01 and 1 Torr.

$\zeta/\rho \to 0$ as $P_2 \to 0$, the value of $\omega L_2/V_2^2$ does not stay constant when P_2 grows. This is probably the result of discharge constriction due to gas heating at higher pressure and may also be due to the skin effect, both being more pronounced at higher discharge power. Both effects decrease the discharge channel cross section and move it closer to the primary coil winding, finally resulting in a rising coupling coefficient and discharge voltage V_2. Visual contraction with growing RF power could be seen in our experiments at higher argon pressure. This phenomena of discharge constriction is well known in DC discharges at high current and gas pressure.

A third way of finding ω/ν_{eff} comes directly from equation (3).

$$\omega/\nu_{eff} = \xi/\rho - (\xi + \rho^2)/k^2 X_0 \rho. \qquad (12)$$

Here the coupling coefficient k remains unknown, but since $k < 1$, one can evaluate the lowest possible value of $\nu_{eff-min}$ (at $k = 1$) suggesting:

$$\nu_{eff} > \nu_{eff-min} = \omega[\xi/\rho - (\xi^2 + \rho^2)/X_0\rho]^{-1}. \qquad (13)$$

The calculation of $\nu_{eff-min}$ for $p = 10$ mTorr over the entire interval of discharge power (20 W $\leqslant P_2 \leqslant$ 100 W) gives $\nu_{eff-min}$ between 3.47×10^7 s^{-1} and 3.27×10^7 s^{-1} both of which are just slightly less than $\nu_{eff} = 3.9 \times 10^7$ s^{-1} found from using equations (10) and (11).

The influence of the coupling coefficient k on the inferred value of ν_{eff} is shown in figure 10 where ratios of ω/ν_{eff} calculated using equation (12) are given as function of discharge power for different values assigned to k. Two interesting features can be seen in figure 10. First, for all reasonable values of k (0.3 $\leqslant k \leqslant$ 1.0), in the limit of $P_2 = 0$ the calculated values of ω/ν_{eff} converge well to the value of $\omega/\nu_{eff} = 2.2$ found earlier. Second, if one assumes that the real value of k is that one which provides constant values for the inferred value of ω/ν_{eff} the result would again be $\omega/\nu_{eff} = 2.2$ or $\nu_{eff} = 3.9 \times 10^7$ s^{-1}. Thus, the effective electron collision frequency found in different ways gives a value of $\nu_{eff} \approx 4 \times 10^7$ s$^{-1} \gg \nu_{en} \approx 2 \times 10^6$ s^{-1}. This result suggests some non-collisional dissipation process responsible for RF power

DOCKET ALARM

Explore Litigation Insights

Docket Alarm provides insights to develop a more informed litigation strategy and the peace of mind of knowing you're on top of things.

Real-Time Litigation Alerts

Keep your litigation team up-to-date with **real-time alerts** and advanced team management tools built for the enterprise, all while greatly reducing PACER spend.

Our comprehensive service means we can handle Federal, State, and Administrative courts across the country.

Advanced Docket Research

With over 230 million records, Docket Alarm's cloud-native docket research platform finds what other services can't. Coverage includes Federal, State, plus PTAB, TTAB, ITC and NLRB decisions, all in one place.

Identify arguments that have been successful in the past with full text, pinpoint searching. Link to case law cited within any court document via Fastcase.

Analytics At Your Fingertips

Learn what happened the last time a particular judge, opposing counsel or company faced cases similar to yours.

Advanced out-of-the-box PTAB and TTAB analytics are always at your fingertips.

API

Docket Alarm offers a powerful API (application programming interface) to developers that want to integrate case filings into their apps.

LAW FIRMS
Build custom dashboards for your attorneys and clients with live data direct from the court.

Automate many repetitive legal tasks like conflict checks, document management, and marketing.

FINANCIAL INSTITUTIONS
Litigation and bankruptcy checks for companies and debtors.

E-DISCOVERY AND LEGAL VENDORS
Sync your system to PACER to automate legal marketing.